EPJ Web of Conferences **302**, 03003 (2024) https://doi.org/10.1051/epjconf/202430203003
SNA + MC 2024

Nucleate boiling within a fuel assembly affected by CRUD

Athanasios Mokos[1*], *Yohei* Sato[2], *Bojan* Niceno[2], *Sergey* V. Churakov[1,3] *and Nikolaos* I. Prasianakis[1]
[1]*Laboratory for Waste Management, Paul Scherrer Institute,5232 Villigen PSI, Switzerland*
[2]*Laboratory for Simulation and Modelling, Paul Scherrer Institute,5232 Villigen PSI, Switzerland*
[3]*Institute of Geological Sciences, University of Bern, Switzerland*

Abstract. Power output of nuclear reactor and heat exchange between fuel assembly and the coolant can be severely affected by the presence of CRUD on the cladding of the fuel assembly. To understand the flow and nucleation boiling processes in the presence of CRUD, a Lattice Boltzmann model for the thermal 3D multiphase flow was developed and implemented in a high-performance multi-GPU-parallel code. The model is applied to procedurally generated CRUD-like structures and the emergence of bubbles due to superheat is investigated. The simulations predict a shorter evaporation time within chimney-like structures as well as the emergence of bubbles at the top layer of the CRUD.

1 Introduction

The flow within a nuclear reactor Fuel Assembly (FA) is extremely complex, both due to the phase change of coolant at high pressure and temperature, and due to the geometry of the FA. The fluid transport and the heat exchange are further complicated by the build-up of mineral deposits, commonly referred to as CRUD, around the fuel system [1]. CRUD precipitates from either the cooling system materials or substances inserted to control the nuclear reaction [2]. It is accumulated during operation and is attached on the FA cladding.

The presence of the CRUD has an effect on the power output of the reactor, by changing the heat resistance of the cladding, potentially affecting the safe operating limits of the plant [3]. The chemical, thermal and flow conditions around the cladding also change which can lead to shorter life cycles of fuel rods and increased radioactivity on the rod which can affect its waste treatment [3]. The surface characteristics also change leading to different nucleation site densities than the original cladding [4, 5].

The CRUD consists of multiple layers of deposits formed by different solid phases. It has a complex porous structure with pore size in the micrometre scale [6] formed around nucleation sites on the FA cladding. The flow within the pores is characterised by multiphase

* Corresponding author: athanasios.mokos@psi.ch

heat and mass transfer [7] with sections of the CRUD forming steam chimneys acting as channels for the transport of vapour into the main flow.

This creates a complex flow domain, whose understanding is of paramount importance [8, 9]. Modelling this flow requires millions of computational grid points as it is an inherently 3D structure. Important controlling mechanisms take place in the microscale rather than the macroscale. Taking these into account, this work uses the Lattice Boltzmann (LB) method to simulate the boiling flow within the porous CRUD. LB was selected because of its ability to resolve microscale flows while recovering the Navier-Stokes equations at the macroscale [10, 11]. In addition, due to the simplicity of the algorithm and the locality of its operator, it is very suited for hardware acceleration using Graphics Processing Units (GPUs) [12].

This work describes the LB model specifically developed for the heat and mass transfer running on a multi-GPU computing system. The code has been validated with a heat conduction case shown in Section 3.1. As CRUD tomographs were not readily available for the simulations, an algorithm for porous media generation is employed instead. The resulting domains are then used for investigating the nucleate boiling within and around steam chimneys.

2 Lattice Boltzmann method

2.1 Thermal multiphase model

The LB method used in this paper recovers the Navier-Stokes equations for a continuous fluid through a multi-scale Chapman-Enskog expansion at the macroscopic limit [10, 11, 13]. The method is applied to 3D space through the D3Q27 lattice. This lattice discretises the field through one rest node and 26 lattice directions, which allows the node to interact with its 26 next neighbouring nodes through discrete velocities c.

The discrete interactions are tracked through a density distribution function f, which corresponds to the inter-particle collisions within the fluid. To compute the density distribution function, the Multi-Relaxation-Time (MRT) collision operator is used as it should have more numerical stability for large density ratios [11, 14, 15]. The LB method then solves 7 equations for the first 7 moments of the flow. In addition, two external forces acting on the system are considered:

- Buoyancy force [14]
- Phase interaction force [16]

The external forces are computed for the LB equations using the method of Li et al.[14, 17]. To connect the LB variables to the flow, summations for the macroscopic density and viscosity are used [11, 14]. For the boundaries a method which imposes a density profile on the surface is used [18].

To solve the temperature field, instead of solving a separate density distribution, the following Equation (1) is used for the diffusive interface of multiphase flows [14, 19, 20]:

$$\frac{\partial T}{\partial t} = -\boldsymbol{v} \cdot \nabla T + \frac{1}{\rho c_v} \nabla \cdot (\alpha \nabla \mathrm{T}) - \frac{T}{\rho c_v} \left(\frac{\partial p_{EOS}}{\partial T} \right) \nabla \cdot \boldsymbol{v} \ , \qquad (1)$$

where T is the temperature, $\boldsymbol{v}$ is the velocity, t is the time, ρ is the density, α is the thermal diffusivity, c_v is the heat capacity at constant pressure and p_{EOS} is the pressure calculated from a weakly compressible equation of state. Equation (1) is discretized with the finite difference method, specifically the isotropic central schemes proposed by [21]. The equation of state used to compute the pressure p_{EOS} is the Peng-Robinson equation also used for the LB method [22].

2.2 High performance GPU code

The code used in this project has been internally developed within the Laboratory for Waste Management and is a multi-CPU-GPU Lattice Boltzmann-based code implemented using CUDA C++ in conjunction with a Message Passing Interface (MPI) [12]. The simulations are executed in the CSCS Swiss National Supercomputing Centre using Nvidia P100 GPUs, which allows for simulations with 15×10^6 nodes per GPU. The code has already been used and validated in multiple projects for the simulation of different phenomena such as fuel cells and desalination membranes [12, 23, 24].

The evolution of the density distribution function includes two major steps; collision and streaming, both of which have no time-implicit dependence on neighbouring nodes, rendering the method explicit and hence fully local. This allows for the computations and memory update on each lattice node to be carried out in parallel, eliminating the need to solve an expensive linear system of equations and making it a good fit for the massive parallelization capabilities of the GPU. This holds for the different boundary conditions as well.

To minimize the expensive CPU-GPU interaction, the computational data are entirely transferred to GPU memory at the beginning of the simulation. To ensure computational balance between the nodes, an 1D decomposition scheme is applied along the longest coordinate. Due to the LB computational advantages, the data that needs to be transferred between GPUs is limited; a 2D slice of node points across the decomposed dimension. The data is transferred to other nodes by using the CPU as an intermediate.

3 Results and discussion

3.1 Thermal code validation

The thermal equation is newly implemented in this work, and thus a validation test is conducted. An unsteady conjugate heat conduction problem [25] is presented here as validation and shown in Fig. 1. The flow velocity is set to zero and the nodes are not allowed to move. Instead, a temperature difference is imposed at the left and right boundaries, where θ is a dimensionless temperature. As the simulation progresses, the temperature within the domain gradually changes until it reaches equilibrium. This is achieved at $t = 2\ s$ as shown in Fig. 1. At this point, the inner temperature is linearly decreasing across the domain, with different gradients depending on the thermal diffusivity and conductivity of the fluid. The LB results are in close agreement with the analytical solution [25].

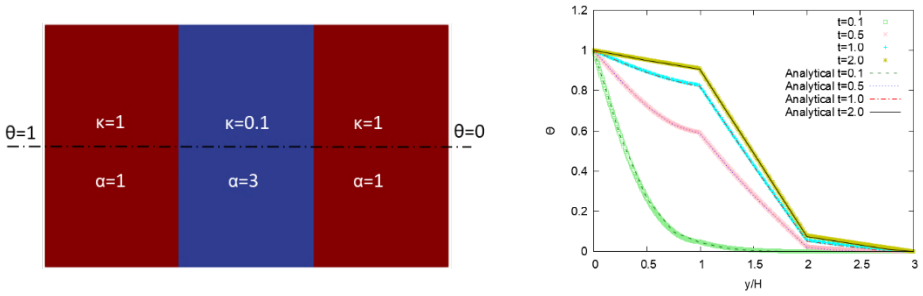

Fig. 1. Simulation domain with different conductivity κ and diffusivity α parameters (left) and comparison with analytical results for different time snapshots (right).

3.2 Generation of porous domain

To model the effect of CRUD, a simulation domain that considers both its porosity and surface roughness is needed. As rods that have developed CRUD and have been removed from the reactor are highly radioactive, it is very difficult to obtain X-ray tomographs of their internal structure. Therefore, in this work, an algorithm will be used to generate synthetic CRUD geometries.

The algorithm consists of two steps: for the internal porous structure and for the surface roughness. For the internal porosity, a 3D domain at the desired dimensions is first created. To each of its nodes is applied a random value generated from a standard Gaussian field varied with a random matrix. Any of the values that are below a certain threshold are the designated as pore spaces. [6].

For the surface roughness, a radially averaged power spectral density algorithm to generate a topography is used [26]. Fig. 2 shows the result of the algorithm on a 400×400×400 domain with a porosity of 0.41.

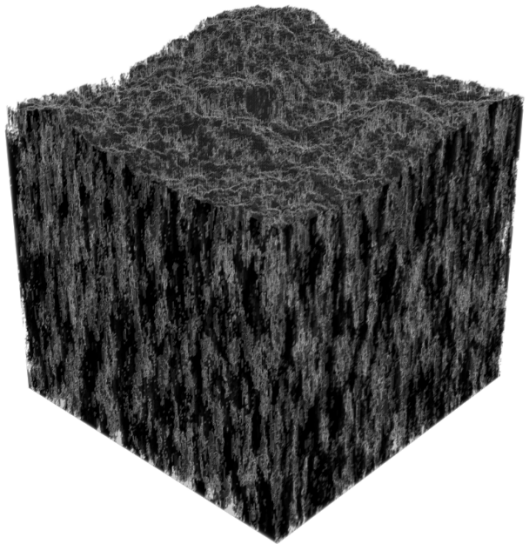

Fig. 2. Generated porous media with a rough surface profile and porosity of 0.41. Black is the CRUD model geometry solid nodes, and grey the free pore-space where multiphase flow takes place.

3.3 Nucleate boiling

The domains generated in section 3.2 and the LB code described in section 3.1 have been used for a nucleate boiling simulation under the effect of CRUD. To simulate the conditions corresponding to a BWR nuclear reactor the following conditions are applied ($T = 295$°C, $P = 70$ bar) with a superheat of 8°C being applied to the middle of the solid phase. The distance between the LB nodes corresponds to 1μm. The dimensionalization of the LB simulation was done based on the controlling dimensionless numbers. The Peng-Robinson parameters were selected from previous literature [17, 27].

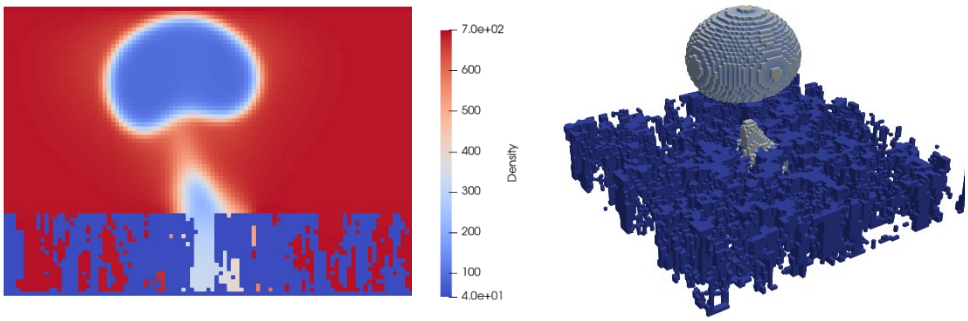

Fig. 3. Simulation of bubble nucleation and departure on a 100×100×70 CRUD domain heated in the middle. Density distribution on a centre plane (left) and a 3D representation of the bubble and CRUD (right).

The first test case concerns a small CRUD domain consisting of 100×100×70 nodes. The superheat was applied in a 20×20×70 area in the centre of the domain and the bubble evolution after 5000 steps are shown in Fig. 3. The increased temperature leads to a drop in density in the middle chimney and the nucleation of a bubble which departs to an outlet on the top as seen in Fig. 4. The fluid within the chimney remains at a low density.

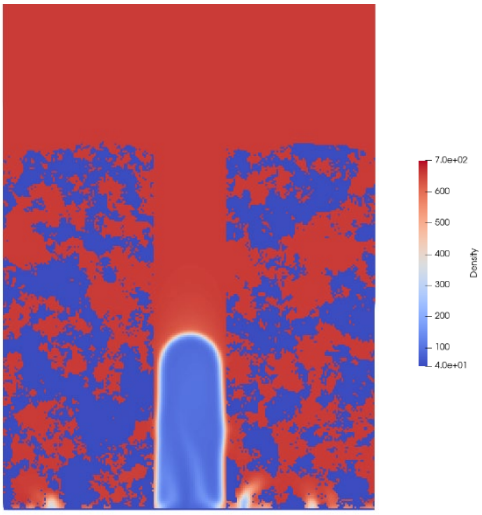

Fig. 4. Simulation of bubble nucleation on a 400x400x400 domain with a chimney of radius 20 at the middle showing the density distribution on a centre plane

To demonstrate the effect of the chimney structure, the structure shown in Fig. 2 is modified with a cylindrical chimney structure of radius 20 LB nodes. The superheat is applied throughout the bottom of the domain. Fig. 4 shows the nucleation of the bubble due to the water boiling. The main bubble has formed within the chimney structure, unobstructed by the porous CRUD, where only smaller bubbles have formed.

To fully utilize the high-performance GPU code, we use a large-scale domain composed of 0.576 billion grid points with a size of 1200×1200×400, which was computed with 24 parallel GPUs at CSCS. The superheat was fully applied to both the CRUD and the bottom of the computational domain, and an outlet boundary is used to the top. As shown in Fig. 5, the superheat causes a drop in density near the top of the porous media, representing the

nucleation of multiple bubbles. These emerge from the pores on the top layer of the CRUD, with larger pores allowing for larger bubbles.

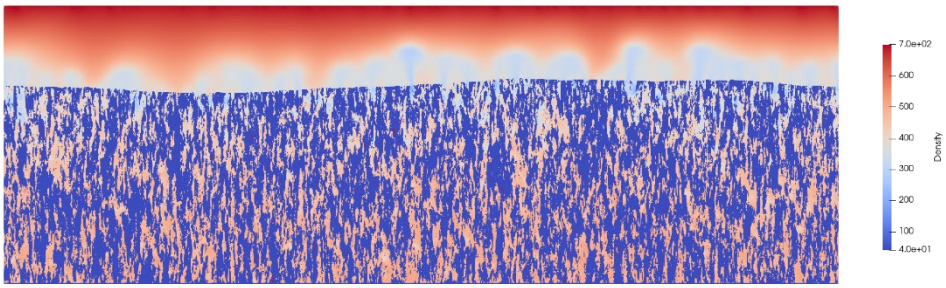

Fig. 5. Density distribution on a sliced plane at 70'000 LB time steps for the simulation of nucleate boiling on a 1200×1200×400 CRUD domain.

4 Conclusions

This work demonstrates the application of a multiphase LB code for the pore scale modelling of the flow within a nuclear reactor. A thermal model was validated and implemented in a high performance, multi-GPU LB code. An algorithm was used to generate porous domains resembling CRUD, which were used with the LB model to simulate bubble nucleation. The results suggest a shorter evaporation time within the steam chimneys as well as the emergence of bubbles at the top layer of the CRUD. Future work will focus on identifying the nucleation site density for different heating conditions under the effect of CRUD.

The authors would like to thank Swissnuclear for providing funding for this research under the project LSM_22_02. We would also like to thank the CSCS Swiss National Supercomputing Centre for providing the computational facilities for the simulations in this work under the project s1155.

References

1. D.Y. Yeo and H.C. No, Int J Heat Mass Tran, **108**: p. 868-879 (2017)
2. I. Dumnernchanvanit, *Characterization and Mitigation of CRUD at Pressurized Water Reactor Conditions*, in *Nuclear Science and Engineering*. 2017, Massachusetts Institute of Technology. p. 467.
3. J. Deshon, *PWR axial offset anomaly (AOA) guidelines, revision 1*. 2004, EPRI: Palo Alto, CA.
4. T. Hibiki and M. Ishii, Int J Heat Mass Tran, **46**: p. 2587-2601 (2003)
5. A. Mokos, et al., Int J Heat Mass Tran, **under review** (2023)
6. C. Xue, et al., Journal of Nuclear Materials, **568**: p. 153899 (2022)
7. B.G. Park, et al., Journal of Nuclear Materials, **512**: p. 100-117 (2018)
8. Y. Sato and B. Niceno, Int J Heat Mass Tran, **125**: p. 876-890 (2018)
9. Y. Sato and B. Niceno, Int J Heat Mass Tran, **105**: p. 505-524 (2017)
10. Y.-H. Qian, D. d'Humières, and P. Lallemand, EPL (Europhysics Letters), **17**(6): p. 479 (1992)
11. P. Lallemand and L.-S. Luo, Phys Rev E, **61**(6): p. 6546-6562 (2000)
12. M.A. Safi, N. Prasianakis, and S. Turek, Comput Math Appl, **73**(3): p. 520-536 (2017)
13. D.A. Wolf-Gladrow, Lect Notes Math, **1725**: p. 1-13 (2000)
14. Q. Li, et al., Int J Heat Mass Tran, **85**: p. 787-796 (2015)
15. L.-S. Luo, et al., Phys Rev E, **83**(5): p. 056710 (2011)

16. X. Shan, Phys Rev E, **73**(4): p. 047701 (2006)
17. Q. Li, K.H. Luo, and X.J. Li, Phys Rev E, **87**(5): p. 053301 (2013)
18. R. Benzi, et al., Phys Rev E, **74**(2) (2006)
19. D.M. Anderson, G.B. McFadden, and A.A. Wheeler, Annual Review of Fluid Mechanics, **30**(1): p. 139-165 (1998)
20. G. Hazi and A. Markus, Int J Heat Mass Tran, **52**(5): p. 1472-1480 (2009)
21. T. Lee and C.-L. Lin, J Comput Phys, **206**(1): p. 16-47 (2005)
22. D. Peng and D.B. Robinson, Ind Eng Chem Fund, **15**(1): p. 59-64 (1976)
23. M.A. Safi, et al., Int J Heat Mass Tran, **115**: p. 238-249 (2017)
24. T. Jaeger, et al., Membranes, **12**(11) (2022)
25. H. Karani and C. Huber, Phys Rev E, **91**(2) (2015)
26. M.M. Kanafi and A.J. Tuononen, Tribol Int, **107**: p. 240-249 (2017)
27. P. Yuan and L. Schaefer, Physics of Fluids, **18**(4) (2006)